Schizophrenia Bulletin vol. 43 no. 5 pp. 1090–1099, 2017
doi:10.1093/schbul/sbx052
Advance Access publication May 16, 2017

Aberrant White Matter Microstructure in Children and Adolescents With the Subtype of Prader–Willi Syndrome at High Risk for Psychosis

Akvile Lukoshe[1,2], Gerbrich E. van den Bosch[3], Aad van der Lugt[4], Steven A. Kushner[5], Anita C. Hokken-Koelega[1,2,7], and Tonya White[*,4,6,7]

[1]Dutch Growth Research Foundation, Rotterdam, The Netherlands; [2]Department of Pediatrics, Erasmus Medical Centre Rotterdam/Sophia Children's Hospital Rotterdam, Rotterdam, The Netherlands; [3]Intensive Care and Department of Pediatric Surgery, Erasmus MC-Sophia Children's Hospital, Rotterdam, The Netherlands; [4] Department of Radiology, Erasmus Medical Centre Rotterdam, Postbus 2040, 3000 CA Rotterdam, The Netherlands; [5]Department of Psychiatry, Erasmus Medical Centre Rotterdam, Rotterdam, The Netherlands; [6]Department of Child and Adolescent Psychiatry, Erasmus Medical Centre Rotterdam—Sophia Children's Hospital, Rotterdam, The Netherlands

[7]These authors contributed equally to the article.

*To whom correspondence should be addressed; tel: +31-0-10-703-70-72, e-mail: t.white@erasmusmc.nl

Prader–Willi Syndrome (PWS) is a complex neurogenetic disorder caused by loss of the paternal 15q11.2–q13 locus, due to deletion (DEL), maternal uniparental disomy (mUPD), or imprinting center defects. Individuals with mUPD have up to 60% risk of developing psychosis in early adulthood. Given the increasing evidence for white matter abnormalities in psychotic disorders, we investigated white matter microstructure in children and adolescents with PWS, with a particular emphasis on the DEL and mUPD subtypes. Magnetic resonance diffusion weighted images were acquired in 35 directions at 3T and analyzed using fractional anisotropy (FA), mean, axial, and radial diffusivity (MD, AD, RD) values obtained by tract-based spatial statistics (TBSS) in 28 children and adolescents with PWS and 61 controls. In addition, we employed a recently developed white matter pothole approach, which does not require local FA differences to be spatially co-localized across subjects. After accounting for age and gender, individuals with PWS had significantly lower global FA and higher MD, compared with controls. Individuals with mUPD had lower FA in multiple regions including the corpus callosum, cingulate, and superior longitudinal fasciculus and larger potholes, compared with DEL and controls. The observed differences in individuals with mUPD are similar to the white matter abnormalities in individuals with psychotic disorders. Conversely, the subtle white matter abnormalities in individuals with DEL are consistent with their substantially lower risk of psychosis. Future studies to investigate the specific neurobiological mechanism underlying the differential psychosis risk between the DEL and mUPD subtypes of PWS are highly warranted.

Keywords: Prader–Willi syndrome/15q11–q13/structural connectivity/neurodevelopmental disorders/psychosis

Introduction

Prader–Willi Syndrome (PWS) is a rare and poorly understood neurodevelopmental disorder that affects 1 in 15 000 live births. PWS is caused by the loss of function of paternally inherited genes on the long arm of chromosome 15q11–q13 due to either deletion (DEL),[1] maternal uniparental disomy (mUPD),[2] unbalanced translocation, or imprinting center defects.[3] PWS is characterized by pre- and postnatal hypotonia, short stature, endocrine problems, hyperphagia, temper tantrums, skin picking, dysmorphic facial features, high pain threshold, and developmental delays.[4] In addition, individuals with PWS carry a high risk of psychosis, especially those with mUPD being at a much higher risk than those with DEL (up to 60% compared to 20%, respectively).[5–7]

The underlying neurobiology by which individuals with PWS, and especially those with mUPD, are at-risk for psychosis remains largely unknown. However, copy number variants within the 15q11–q13 locus have been strongly associated with an increased risk of schizophrenia and autism, including microdeletions of 15q11.2 and 15q13.3, as well as maternally inherited duplications of the 15q11–q13 Angelman Syndrome/PWS locus.[8–10] Although the precise neurobiological mechanisms have yet to be elucidated, these findings suggest a remarkable convergence among the pathways underlying psychosis, autism, intellectual disability, and PWS.[11,12]

White matter abnormalities have been widely implicated in the aetiology of several psychiatric disorders, including schizophrenia,[13,14] bipolar disorder,[15] intellectual disability, and autism.[16] Aberrant white matter microstructure has been found in individuals with prodromal symptoms and ultra-high risk of conversion to schizophrenia, for whom an impairment of white matter microstructure predicted both a worsening of cognitive outcome[17,18] and increased risk for conversion to schizophrenia.[19] This suggests that white matter development precedes the emergence of psychiatric disorders and might therefore contribute to the development of psychopathology. Consequently, an investigation of white matter microstructure in children and young adolescents with PWS, but prior to the onset of psychosis, might provide unique insights regarding the pathophysiology of psychosis in PWS.

To date, no DTI studies have ever been conducted in children and adolescents with PWS. One previous DTI study was conducted in adults with PWS,[20] however genetic subtypes and psychiatric history were not included as covariates.

Although there is considerable evidence that white matter microstructure abnormalities factor prominently in the development of psychiatric disorders, the spatial location of white matter changes appear to be quite heterogeneous, even among individuals with similar diagnoses.[21] Discrepancies can be partially explained by voxel-based analyses that assume the co-localization of white matter abnormalities in the majority of patients. For example, white matter abnormalities have been shown to be not overlapping in children with early-onset schizophrenia by employing the "pothole approach," which does not assume co-localization of white matter abnormalities, indicating that conventional DTI analysis might be insensitive to more global but variably localized pathology.[22,23]

In the current study, we explored the properties of white matter microstructure by diffusion tensor imaging (DTI) in children and adolescents with PWS and no prior history of psychosis, employing both conventional voxel-based DTI analyses and the global pothole method. We hypothesized that white matter microstructure would be reduced in individuals with PWS, compared to controls, as developmental delay is prominent in all individuals with PWS. In addition, we expected the differences to be more pronounced in individuals with mUPD than in those with DEL, due to their increased risk for psychosis. In addition, we expected to find aberrant white matter microstructure in individuals with mUPD in the following regions of interest (ROIs): cingulum, corpus callosum, anterior corona radiata, and fronto-occipital fasciculus, compared to both controls and individuals with DEL, as these brain regions are among the most well-replicated across studies of white matter microstructure in case–control cohorts of psychosis.[19,21,24,25] Finally, we made an a priori designation of primary white matter tracts for which brain imaging studies of patients with schizophrenia have consistently shown no differences, namely pontine crossing tract, corticospinal tract, medial lemniscus, and superior and inferior cerebellar peduncles.

Methods

The study population consisted of 38 children and adolescents with PWS recruited from within Dutch PWS Cohort Study.[26,27] Patients fulfilled the following criteria: (1) genetically confirmed PWS, (2) age 6–25 years, (3) no history of neurological or psychotic symptoms, and (4) no history of psychotropic medication.

Seventy-four age- and sex-matched, typically developing children and adolescents were included as the control group, fulfilling the following inclusion criteria: (1) age 6–25 years, (2) without neurological or psychiatric history, and (3) without a history of psychotropic medication.

The study was approved by the Medical Ethical Committee of the Erasmus MC Rotterdam, The Netherlands. Written informed consent was obtained in all cases from the caregivers and children older than 12 years of age. Informed assent was obtained in children younger than 12 years of age.

Procedure

Prior to the MRI scan, all controls underwent a habituation session in a mock scanner.[28] For subjects with PWS, similar habituation sessions resulted in either neutral or overtly negative anxiogenic effects, therefore they were acclimated to the MRI environment by providing a digital audio recording of MRI scanner noise prior to their visit, as well as a short demonstrative explanation in the MRI suite. This proved to be a more successful approach for PWS patients. For both controls and children with PWS, a caregiver was encouraged to remain in the MRI suite, close to the child, throughout the imaging session.

MRI Acquisition

Imaging was performed on a 3T GE 750 Discovery MRI scanner (General Electric), using an 8-channel head coil. The DTI sequence consisted of a 35-direction echo planar imaging (EPI) sequence using the following parameters: TR = 11 000 ms, TE = 80.8 ms, NEX = 1, flip angle = 90, b = 0 and 1000 s/mm^2, matrix 128 × 128 and an isotropic voxel resolution of 2.0 × 2.0 × 2.0 mm^3. The b = 0 s/mm^2 was acquired 3 times. The total scan time for the DTI sequence was 7 min 40 s.

Image Preprocessing

All DTI data were preprocessed by the FMRIB's Diffusion Toolbox (FDT) from the FMRIB's freely available Software Library (FSL, http://www.fmrib.ox.ac.uk/fsl). Images were corrected for eddy currents and

simple head motion artifacts by aligning to the corresponding nondiffusion weighted (b_0) image.[29] Nonbrain tissue was removed from the b_0 images by using FSL's Brain Extraction Tool (BET).[30] Tensor models were fitted to the diffusion-weighted images at each voxel using a least-squares multivariate linear fitting algorithm, after which the voxelwise values of fractional anisotropy (FA) as well as mean, axial and radial diffusivity (MD, AD, RD, respectively) were calculated.[29] Global FA, MD, AD, and RD values were defined as sum of all white matter voxels, defined by the John Hopkins atlas. All images were individually inspected for alignment issues or corruption due to motion. Root mean square (RMS) was estimated, based on translations and rotations (in mm) and a cut-off value of 1 mm was set.

Tract-Based Spatial Statistics

Voxelwise whole-brain analysis of FA images was performed using tract-based spatial statistics (TBSS) tool of FSL.[29] All subjects were iteratively aligned to estimate the minimum warping necessary for co-registration. The image that required the least warping was set as a target image. The target image was aligned to standard space using the Montreal Neurological Institute (MNI152) template, and every comparison image was subsequently transformed to $1 \times 1 \times 1$ mm^3 MNI152 standard space by applying a nonlinear transformation (FNIRT). All DTI images were merged into a single 4D file, which was used to create a mean FA skeleton with an FA threshold of 0.3. Finally, the aligned FA images of each participant were projected onto the mean skeleton to create individual skeletonized FA maps for each subject.

To examine group-wise differences, skeletonized FA data were analyzed using a nonparametric voxel-wise algorithm based on permutation test theory. The analysis was performed using the FSL randomize tool, which utilizes 5000 random permutations with 2 contrasts (control > PWS and PWS > control) with age and gender as covariates. Threshold-free cluster enhancement (TFCE) was used to correct for multiple testing at $P < .05$. Similar analyses were performed to investigate the differences between children with DEL or mUPD vs controls, and the differences between the DEL and mUPD subgroups. All comparisons were corrected for age and gender.

Sensitivity TBSS Analysis

In order to ensure that differences in age and gender between groups do not bias the results, sensitivity TBSS analysis was conducted in patients and a subset of age- and gender matched controls.

ROI Analysis

The Johns Hopkins University (JHU) white matter atlas[31] was co-registered with the DTI images in standard MNI space. Mean FA, MD, AD, and RD was extracted from a pre-defined set of ROIs (corpus callosum, cingulum, fronto-occipital fasciculus, longitudinal fasciculus, and anterior corona radiata), together with negative controls defined based on their lack of association with schizophrenia and psychosis (pontine crossing tract, corticospinal, medial lemniscus, inferior and superior cerebellar peduncles).

Pothole Analysis

Each subject's aligned FA data (nonlinearly registered into MNI space) was fed into an in-house Matlab program (R2012b, Mathworks) in order to quantify the number of white matter potholes along the major WM tracts.[22] The mean and standard deviation images were generated by pooling controls and patients together. These images were used to create voxel-wise z-images for individual subject. To ensure that only white matter regions were included, each image was masked with the white matter tracts defined by John Hopkins University (JHU) white matter atlas. Further, each image was masked with a z threshold of $z < -2$. The individual masked z-images were searched for contiguous voxel clusters (potholes) falling below a z-threshold of −2 and greater than a specified cluster size (either 50, 100, 150, or 200 voxels).

Results of global FA and MD values and white matter tract potholes were exported to SPSS (version 21, IBM Corporation) for statistical analyses. Global FA values and number of potholes were pooled between the right and left hemispheres due to absence of any a priori hypotheses regarding lateralization. Quade's test, a nonparametric alternative to covariance analysis, was performed with age and gender as covariates. Benjamini–Hochberg false discovery rate (FDR) correction of 0.05% was applied to correct for multiple testing across the white matter tracts. After correction for multiple testing, pairwise comparisons were performed for significant main effects. Bonferroni correction was applied ($P_{corr} = P \times 3$) for group comparisons and adjusted P_{corr} values are reported unless indicated otherwise. The significant P_{corr} value was set at .05.

Results

Participants

Subject data are presented in table 1 (demographics) and supplementary figure 1 (age distribution). Ten patients and 13 healthy controls were excluded from further analysis due to excessive motion, resulting in 28 patients and 61 controls.

No differences were found in gender distribution between the groups. There was a marginally significant difference in age between groups ($P < .05$), for which pairwise comparisons revealed that patients with the DEL genotype were significantly older than the control group.

Table 1. Demographic Data of the Participants

	PWS			
	DEL	mUPD	Control	*P* value
Age (years)	14.4 (4.1)	11.8 (3.5)	11.7 (2.6)	<.05
Age range (years)	8.4–23.1	6.9–18.4	7.1–17.9	
Sample size (*N*)	15	13	61	
Gender (*N*)				ns
Male	7	3	28	
Female	8	10	33	
Age at start of GH treatment	6.6 (3.5)	4.6 (2.9)	n/a	ns
Total IQ score	68.6 (14.6)	70.4 (12.8)	n/a	ns
Verbal IQ	3.9 (3.2)	4.5 (2.7)	n/a	ns
Performance IQ	4.7 (2.6)	4.8 (2.7)	n/a	ns
Psychiatric history	0	2[a]	n/a	
Use of psychotropic medication	0	0	n/a	

Note: n/a, not applicable.
[a]Two children were diagnosed with autism spectrum disorders prior to MRI study.

No significant differences were observed in the other pairwise comparisons (mUPD vs controls, mUPD vs DEL).

Diffusivity Measures: Global and ROI Analyses

PWS Vs Controls. Global FA and MD measures, as well as those of ROIs according to the JHU atlas, are presented in table 2. Individuals with PWS had lower global FA compared to controls ($P < .001$). ROI analyses revealed lower FA in the corpus callosum ($P < .001$), superior longitudinal fasciculus ($P < .001$), anterior corona radiata ($P < .01$), cingulum ($P < .01$), and superior fronto-occipital fasciculus ($P < .05$). No differences were found in any of the negative controls.

Individuals with PWS had higher global MD compared to controls ($P < .001$). ROI analyses revealed higher MD, AD, and RD in anterior corona radiata ($P < .05$) and superior fronto-occipital fasciculus ($P < .05$); higher MD and RD in the corpus callosum ($P < .001$), superior longitudinal fasciculus ($P < .01$), and higher RD in cingulum ($P < .001$). Of the negative control tracts, inferior cerebellar peduncle had significantly higher MD (<.001), in combination with higher AD ($P < .001$). Pontine crossing tract and medial lemniscus had significantly higher RD ($P < .001$), without differences in MD, and corticospinal tract had higher RD and AD values ($P < .05$), without significant differences in MD.

Pairwise Comparisons.

mUPD vs Controls Global FA was significantly lower in mUPD compared to controls ($P < .001$). In the ROI-specific analysis, FA was significantly lower in corpus callosum ($P < .001$), superior longitudinal fasciculus ($P < .01$), anterior corona radiata ($P < .01$), cingulum ($P < .01$), and superior fronto-occipital fasciculus ($P < .01$).

Global MD was significantly higher in mUPD compared to controls ($P < .001$). In the ROI analysis, MD and RD, but not AD, were significantly higher in corpus callosum ($P < .001$), superior longitudinal fasciculus ($P < .01$), anterior corona radiata ($P < .01$) and superior fronto-occipital fasciculus ($P < .001$). Superior fronto-occipital fasciculus had also significantly higher AD ($P < .001$).

DEL Vs Controls Global FA was similar between DEL and controls. ROI analyses revealed a difference only in the superior longitudinal fasciculus ($P < .05$).

Global MD was significantly higher in DEL ($P < .05$). Anterior corona radiata and superior fronto-occipital fasciculus had significantly higher MD ($P < .05$ and $P < .001$, respectively), AD ($P < .01$ and $P < .001$, respectively) and RD ($P < .01$ and $P < .05$, respectively).

mUPD Vs DEL Global FA was significantly lower in mUPD compared to DEL ($P < .05$). ROI-specific analyses demonstrated significantly lower FA in mUPD across corpus callosum ($P < .01$), anterior corona radiata ($P < .05$), cingulum ($P < .01$), and superior fronto-occipital fasciculus ($P < .05$).

No differences in tract-specific MD and AD were observed between mUPD and DEL. Higher RD was found in corticospinal tract in patients with mUPD ($P < .05$).

Tract-Based Spatial Statistics

PWS Vs Controls. We found clusters with significantly lower FA in individuals with PWS, compared to controls in the corpus callosum, cingulum, superior longitudinal fasciculus, retrolenticular part of internal capsule, superior corona radiata and external capsule (figure 1, part I).

Pairwise Comparisons.

mUPD Vs Controls Individuals with mUPD had multiple large clusters with lower FA compared to controls: corpus callosum, cingulum, anterior corona radiata, superior and inferior longitudinal fasciculi, retrolenticular part of internal capsule, anterior limb of internal capsule, and external capsule (figure 1, part II).

Table 2. Global Fractional Anisotropy and Mean, Axial, and Radial Diffusivity Measures in Children mUPD and DEL Subtypes of PWS and Controls

	PWS						Between Groups		Pairwise Comparisons		
	mUPD		DEL		Control			FDR Corrected	mUPD Vs HC	DEL Vs HC	mUPD Vs DEL
	Mean	SD	Mean	SD	Mean	SD	*P* value	*P* value	*P* value	*P* value	*P* value
Regions of interest											
Global measures											
FA	0.417	0.015	0.439	0.013	0.441	0.018	**<.0001**	**<.0001**	**<.0001**	ns	**.036**
MD	0.919	0.041	0.885	0.035	0.863	0.031	**<.0001**	**<.0001**	**<.0001**	**.013**	ns
Corpus callosum											
FA	0.466	0.024	0.512	0.019	0.513	0.023	**<.0001**	**<.0001**	**<.0001**	ns	**.001**
MD	1.040	0.069	0.981	0.064	0.955	0.062	**<.0001**	**<.0001**	**<.0001**	ns	ns
AD	1.578	0.065	1.567	0.075	1.543	0.064	.09	ns			
RD	0.771	0.073	0.688	0.062	0.661	0.063	**<.0001**	**<.0001**	**<.0001**	ns	ns
Superior longitudinal fasciculus											
FA	0.393	0.016	0.404	0.018	0.418	0.026	**<.0001**	**<.0001**	**.002**	**.016**	ns
MD	0.763	0.029	0.742	0.016	0.740	0.024	**.005**	**.009**	**.005**	ns	ns
AD	1.101	0.036	1.078	0.027	1.094	0.030	.33	ns			
RD	0.595	0.027	0.574	0.021	0.564	0.029	**.001**	**.002**	**.005**	**.012**	ns
Anterior corona radiata											
FA	0.348	0.019	0.376	0.024	0.378	0.026	**.001**	**.002**	**<.0001**	ns	**.026**
MD	0.908	0.083	0.876	0.075	0.839	0.043	**<.0001**	**<.0001**	**.001**	**.022**	ns
AD	1.242	0.093	1.236	0.087	1.200	0.047	**.004**	**.011**	ns	.007	ns
RD	0.741	0.079	0.697	0.072	0.658	0.046	**<.0001**	**<.0001**	**.001**	**.008**	ns
Cingulum											
FA	0.304	0.028	0.349	0.024	0.337	0.029	**.002**	**.002**	**.004**	ns	**.003**
MD	0.826	0.032	0.800	0.020	0.806	0.027	.96	ns			
AD	1.099	0.031	1.118	0.038	1.114	0.032	.19	ns			
RD	0.689	0.036	0.641	0.027	0.652	0.034	**<.0001**	**<.0001**	**<.0001**	ns	ns
Superior fronto occipital fasciculus											
FA	0.366	0.038	0.408	0.035	0.402	0.034	**.004**	**.004**	**.006**	ns	ns
MD	0.850	0.170	0.789	0.106	0.729	0.025	**<.0001**	**<.0001**	**<.0001**	**<.0001**	ns
AD	1.176	0.165	1.150	0.100	1.075	0.036	**<.0001**	**<.0001**	**.001**	**<.0001**	ns
RD	0.687	0.173	0.608	0.112	0.557	0.033	**.001**	**.002**	**.005**	**.012**	ns
Negative control tracts											
Pontine crossing tract											
FA	0.382	0.041	0.360	0.035	0.382	0.030	.18	ns			
MD	0.884	0.096	.930	0.112	0.863	0.082	.27	ns			
AD	1.229	0.111	1.289	0.136	1.213	0.095	.20	ns			
RD	0.711	0.093	0.750	0.108	0.688	0.079	**<.0001**	**<.0001**	**.001**	**.008**	ns
Corticospinal											
FA	0.282	0.034	.285	0.056	0.291	0.035	.65	ns			
MD	1.484	0.311	1.438	0.294	1.299	0.202	.038	ns			
AD	1.853	0.330	1.816	0.316	1.665	0.227	**.021**	**.046**	ns	**.024**	ns
RD	1.300	0.302	1.249	0.285	1.116	0.191	**.01**	**.03**	**.01**	ns	.021
Medial lemniscus											
FA	0.437	0.036	0.441	0.022	0.444	0.019	.65	ns			
MD	0.780	0.093	0.778	0.050	0.742	0.029	**.038**	ns			
AD	1.167	0.174	1.163	0.081	1.114	0.034	.12	ns			
RD	0.587	0.058	0.586	0.038	0.555	0.030	**<.0001**	**<.0001**	**<.0001**	.002	ns
Inferior cerebellar peduncle											
FA	0.366	0.028	0.357	0.025	0.355	0.025	.31	ns			
MD	0.864	0.060	0.837	0.062	0.816	0.027	**<.0001**	**<.0001**	**.002**	**.012**	ns
AD	1.211	0.095	1.177	0.083	1.137	0.040	**<.0001**	**<.0001**	**.009**	**.003**	ns
RD	0.690	0.045	0.667	0.053	0.656	0.029	.16	ns			
Superior cerebellar peduncle											
FA	0.462	0.020	0.471	0.014	0.469	0.025	.33	ns			
MD	1.324	0.092	1.318	0.076	1.278	0.093	.20	ns			
AD	1.911	0.109	1.912	0.095	1.847	0.108	0.039	ns	**ns**	.049	ns
RD	1.030	0.089	1.020	0.071	0.994	0.091	0.051	ns			

Note: FA, fractional anisotropy; MD, mean diffusivity; AD, axial diffusivity; RD, radial diffusivity; FDR, false discovery rate; PWS, Prader–Willi syndrome; mUPD, maternal uniparental disomy; DEL, deletion; HC, controls; SD, standard deviation. Results are corrected for age and gender. MD, AD, and RD are expressed as ($\times 10^{-3}$) mm^2/s. Values in bold are the significant *P* values.

DEL Vs Controls Individuals with DEL had no clusters with lower FA compared to controls (figure 1, part III).
mUPD Vs DEL Individuals with mUPD had lower FA across multiple brain regions, compared to DEL. These regions included the corpus callosum, cingulum, anterior and superior corona radiata, external capsule, posterior thalamic radiation, and superior longitudinal fasciculus (figure 1, part IV).

Sensitivity TBSS Analysis

Patient demographics and results are presented in supplementary table 1 and supplementary figure 2.

White Matter Potholes

Individuals with PWS had significantly more potholes than controls, a difference which persisted across a wide range of pothole sizes: 50, 100, 150, or 200 contiguous voxels ($P < .0001$, table 3 and figure 2). Subtype-specific pairwise comparisons revealed that the largest differences were observed between individuals with mUPD and controls in each of the 4 size categories ($P < .0001$). Moreover, in contrast to the results of the conventional analyses of global FA measures and TBSS, significant differences were also observed between individuals with DEL and controls ($P < .01$ in all 4 pothole size categories). Notably however, among the largest sizes (150 and

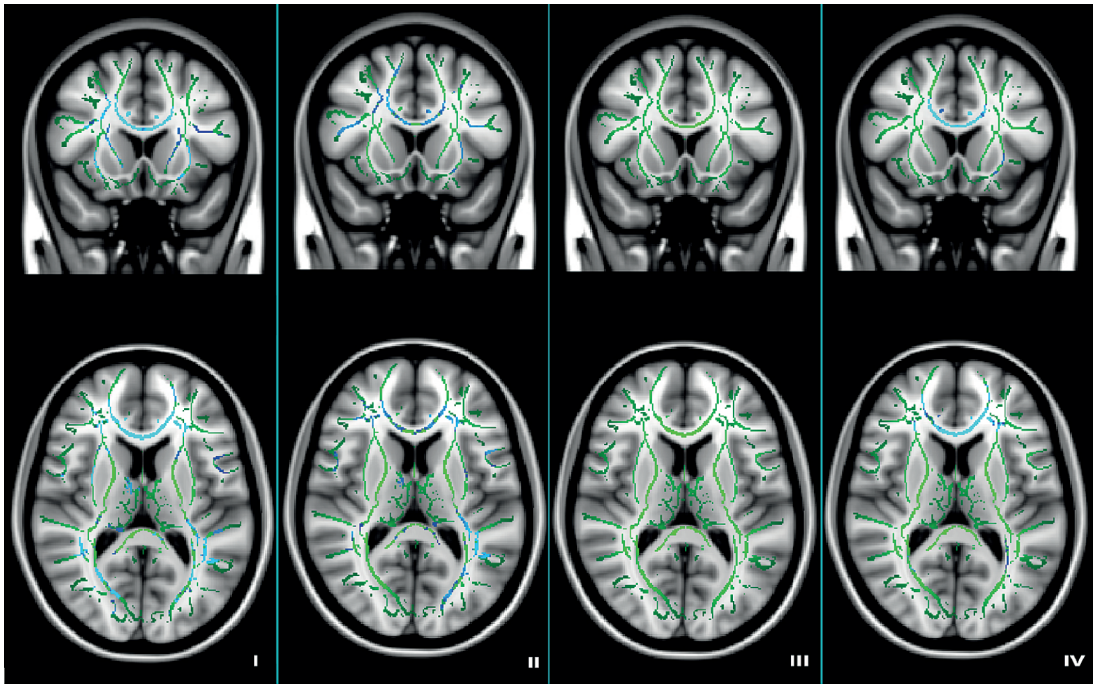

Figure 1. Tract-based spatial statistics results in children with PWS and controls. Results are corrected for age and gender. Image coordinates X91 Y142 Z83, upper row—coronal view; bottom row—horizontal view. Green: white matter skeleton; light blue—clusters with lower FA ($P < .05$); dark blue—clusters with lower FA ($P < .001$). (I) PWS vs controls; (II) mUPD vs controls; (III) DEL vs controls, and (IV) mUPD vs DEL.

Table 3. Number of Potholes per Pothole Size Category in Children with mUPD and DEL Subtypes and Controls.

	PWS						Between Groups		Pairwise Comparisons		
	mUPD		DEL		Control			FDR Corrected	mUPD Vs HC	DEL Vs HC	mUPD Vs DEL
	Mean	SD	Mean	SD	Mean	SD	*P* value	*P* value	*P* value	*P* value	*P* value
Number of potholes											
Pothole size 50	74.9	12.9	52.4	15.7	36.6	18.7	**<.0001**	**<.0001**	**<.0001**	**.001**	ns
Pothole size 100	39.7	6.9	25.5	10.1	16.8	11.2	**<.0001**	**<.0001**	**<.0001**	**.001**	ns
Pothole size 150	25.5	6.2	14.9	7.3	9.6	6.5	**<.0001**	**<.0001**	**<.0001**	**.005**	**.014**
Pothole size 200	18.8	5.6	10.9	5.9	6.1	5.1	**<.0001**	**<.0001**	**<.0001**	**.001**	**.048**

Note: FDR, false discovery rate; PWS, Prader–Willi syndrome; mUPD, maternal uniparental disomy; DEL, deletion; HC, controls; SD, standard deviation. Results are corrected for age and gender.

200 contiguous voxels) individuals with mUPD had significantly more potholes compared to individuals with DEL ($P < .05$) (figure 3).

Discussion

This is the first study investigating white matter microstructure in children and adolescents with PWS. We found reduced white matter microstructure in young individuals with PWS in most of the major white matter tracts, including the corpus callosum, cingulum, superior longitudinal fasciculus, anterior and superior corona radiata, as well as retrolenticular part of internal capsule and external capsule. Post hoc analyses revealed that these findings were disproportionately present in the mUPD subtype of PWS. Individuals with mUPD had significantly lower FA and higher RD as well as AD in corpus callosum, superior longitudinal fasciculus, anterior corona radiata, cingulum and superior fronto-occipital fasciculus. In contrast, individuals with DEL had no tract-based clusters with significant alterations in FA, but had increased RD and AD in superior longitudinal and superior fronto-occipital fasciculi. In pairwise comparisons between the mUPD and DEL subtypes of PWS, global FA was lower in individuals with mUPD, and not in those with DEL, indicating that aberrant white matter microstructure is a widespread phenomenon in mUPD. Analogously, individuals with mUPD tended to have larger potholes compared to individuals with DEL. Furthermore, except for the superior longitudinal fasciculus, all of the tract-based FA differences in the mUPD group were significant compared to both controls as well as DEL. Moreover, no differences in FA were found in any of the white matter tracts designated a priori as regions of no association with schizophrenia. Taken together, individuals with the mUPD subtype of PWS appear to have a highly overlapping burden of white matter pathology as other diseases for which psychosis is a prominent feature, in particular schizophrenia.

Given that individuals with mUPD have a much higher risk for developing psychosis (60%, compared to 20% in DEL[6,32]), it is tempting to speculate that the observed alterations in white matter microstructure may function etiologically in the underlying risk of psychosis. In contrast, the subtype-selectivity of the white matter pathology suggests a much weaker association with developmental delay, which is present in both mUPD and DEL, compared to the highly elevated risk of psychosis

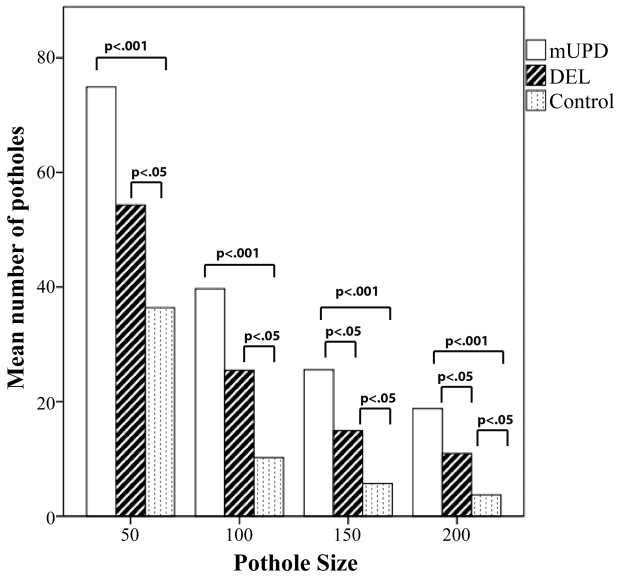

Figure 2. Pothole number per pothole size category in individuals with PWS and controls.

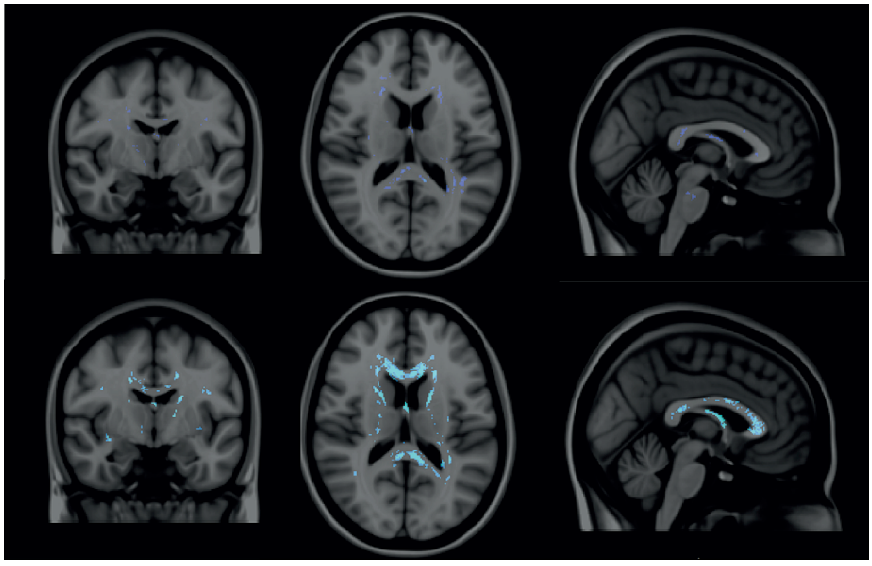

Figure 3. White matter potholes in DEL and mUPD subgroups. Top row: potholes in individuals with DEL. Bottom row: potholes in individuals with mUPD. Dark blue: $P < .05$; light blue: $P < .001$.

in the mUPD subtype. Furthermore, nearly all of the changes observed in mUPD group have been reported and replicated in patients with schizophrenia,[13,14] as well as in individuals at ultra-high risk of psychotic disorders.[17,24,25] In particular, a decrease of FA within the corpus callosum, corona radiata and superior fronto-occipital fasciculus predicted the subsequent conversion to psychosis in those at ultra-high risk.[18,19] It is therefore possible that the aberrant white matter microstructural findings in individuals with mUPD and no prior history of psychosis, are related to their highly elevated risk of conversion to psychosis. Longitudinal follow-up studies will be necessary to examine whether abnormalities in white matter microstructure are sufficient to risk-stratify individuals with PWS regarding their future risk of psychosis.

Central nervous system myelination begins in utero and continues until late adulthood,[33] performed exclusively by oligodendrocytes.[34] Among the genes of the PWS locus, UBE3A is expressed throughout the brain, including neurons and oligodendrocytes,[35] but the gene has a different imprinting status depending on the cell type and time-point in development. In oligodendrocytes of wild-type mice, UBE3A is not imprinted and is thus expressed biallelically.[35] In the mUPD case of PWS, UBE3A is expressed from 2 maternal chromosomes. In contrast, individuals with a deletion of the paternal allele, there is only one active copy of UBE3A present. We would therefore expect large differences in white matter microstructure in individuals with DEL, but not in those with mUPD. However, we observed the opposite effect, thus it is very unlikely that the observed global reduction of white matter microstructure in mUPD is due to abnormal oligodendrocyte function.

Neuronal expression of UBE3A, in contrast to oligodendrocyte expression, is similar in DEL and controls, as the maternal allele is unaffected in DEL, and increased in mUPD, due to presence of 2 maternal alleles, leading to impaired neuronal function.[36] Therefore, the mUPD subtype-specific impairments seem more likely to have arisen from a primary abnormality in neurons which secondarily impacts myelination, rather than directly from a primary oligodendrocyte dysfunction. Consistent with this hypothesis, elegant studies in rodents have provided strong evidence that neuronal input powerfully modulates oligodendrocyte precursor cell proliferation and maturation, and oligodendrocyte myelination.[37–39]

Our findings are consistent with the previous white matter diffusion study in adults with PWS,[20] in which aberrant white matter microstructure was observed in the posterior limb of internal capsule and the splenium of corpus callosum, however subtype analyses were not performed. Our current findings replicate and extend these results, demonstrating the white matter abnormalities primarily arise from the mUPD subtype and are already present in childhood.

Moreover, given that aberrant white matter microstructure has been reported in patients with intellectual disability,[40] our findings might be considered as primarily associated with developmental delay. However, it must be taken into account that although FA is a sensitive marker of white matter microstructure,[41] it does not reflect the nature of white matter microstructure differences, as it driven by myelination, axonal diameter, and packing density as well as axonal organization (crossing or kissing fibers).[42] The additional AD and RD measures suggest a delay in myelination as axial and radial diffusivity decreases during normal brain development.[43] Potential differences in axonal organization in PWS group are likely as well, as it is also shown that change in RD caused change in AD in voxels characterized by crossing fibers[44] All in all, the combination of the results of the present study together with our previous structural imaging findings indicate a global burden of white matter abnormalities that is substantially more severe in individuals with mUPD compared to those with DEL,[45] either due to delayed myelination, differences in axonal properties organization or a combination of these factors.

Interestingly, we found no differences in global FA values and all tracts except superior longitudinal fasciculus between individuals with DEL and controls. Some AD and RD differences were observed, both in tracts of interest and in negative control tracts, which are not associated with psychotic disorders. In contrast, the pothole approach which does not require FA reductions in white matter to be spatially overlapping across individuals[22] did reveal substantial differences between individuals with DEL and controls. This suggests that although distinct from the more severe impairments observed in mUPD, individuals with DEL also show signs of aberrant white matter development which may contribute to their cognitive impairment and increased risk of psychopathology.[5,32]

The mUPD group was closely age-matched to the controls, however the DEL group was significantly older, thereby raising the question of whether the absence of findings in the DEL group might have resulted from a longer duration of white matter development. However, all of the analyses have been reported with the inclusion of a correction for age. Furthermore, we have conducted a supplementary TBSS analysis in a subset of patients and controls, matched for age and gender, and the observed differences between mUPD vs HC as well as DEL vs HC remained significant (supplementary figure 2), therefore confirming that the observed differences are not due to age or gender, but rather due to their diagnostic status.

These results are limited by the small sample size, thus generalization to broader PWS population should be undertaken with great caution. Further, all patients with PWS were receiving treatment with growth hormone (GH) at the time of the study, in accordance with the current standard-of-care guidelines in all individuals with PWS. GH and insulin-like growth factor-1 (IGF-1) have been shown to promote

oligodendrocyte maturation[46] and facilitate myelination.[47] The Dutch randomized control GH trial demonstrated that initiating GH therapy during early life improved cognitive functioning,[48] motor development[26] and adaptive behavior (Lo et al.[49]) in children with PWS. Given that the rate of white matter development is most intensive during the first 5–6 years of life,[34,50,51] it is possible that early treatment with GH, especially when started during the first 2 years of life, could influence white matter formation. Importantly however, since GH therapy is administrated equivalently to patients with mUPD and DEL, the differences in white matter microstructure between these subtypes cannot be explained by GH treatment.

Conclusions

We report impaired white matter tract microstructure in children and adolescents with mUPD, compared to those with DEL and controls. The differences in individuals with DEL compared to controls were less pronounced and evident only when using spatially independent measures. These findings suggest that the high risk of conversion to psychosis in individuals with mUPD might result from an aberrant developmental trajectory of white matter microstructure. Longitudinal follow-up studies are warranted to further clarify the relationship between genetic factors, brain development, and risk of psychotic illness in individuals with PWS.

Supplementary Material

Supplementary data are available at *Schizophrenia Bulletin* online.

Funding

This study was financially supported by Foundation for Prader–Willi Research (FPWR) and Dutch Growth Research Foundation.

Acknowledgments

We would like to thank parents and patients for their participation. We also thank Renske Kuppens, Nienke Bakker, Sinddie Lo, and Marielle van Eekelen with their assistance with the MRI acquisition, Ryan Muetzel for the help with the analyses.

References

1. Ledbetter DH, Riccardi VM, Airhart SD, Strobel RJ, Keenan BS, Crawford JD. Deletions of chromosome 15 as a cause of the Prader–Willi syndrome. *N Engl J Med*. 1981;304:325–329.
2. Nicholls RD, Knoll JH, Butler MG, Karam S, Lalande M. Genetic imprinting suggested by maternal heterodisomy in nondeletion Prader–Willi syndrome. *Nature*. 1989;342:281–285.
3. Buiting K, Saitoh S, Gross S, et al. Inherited microdeletions in the Angelman and Prader–Willi syndromes define an imprinting centre on human chromosome 15. *Nat Genet*. 1995;9:395–400.
4. Cassidy SB, Forsythe M, Heeger S, et al. Comparison of phenotype between patients with Prader–Willi syndrome due to deletion 15q and uniparental disomy 15. *Am J Med Genet*. 1997;68:433–440.
5. Veltman MW, Craig EE, Bolton PF. Autism spectrum disorders in Prader–Willi and Angelman syndromes: a systematic review. *Psychiatr Genet*. 2005;15:243–254.
6. Sinnema M, Boer H, Collin P, et al. Psychiatric illness in a cohort of adults with Prader–Willi syndrome. *Res Dev Disabil*. 2011;32:1729–1735.
7. Verhoeven WM, Tuinier S, Curfs LM. Prader–Willi syndrome: the psychopathological phenotype in uniparental disomy. *J Med Genet*. 2003;40:e112.
8. Stefansson H, Rujescu D, Cichon S, et al.; GROUP. Large recurrent microdeletions associated with schizophrenia. *Nature*. 2008;455:232–236.
9. Rees E, Walters JTR, Georgieva L, et al. Analysis of copy number variations at 15 schizophrenia-associated loci. *Br J Psychiatry.* 2014;204:108–114.
10. Moreno-De-Luca D, Sanders SJ, Willsey AJ, et al. Using large clinical data sets to infer pathogenicity for rare copy number variants in autism cohorts. *Mol Psychiatry*. 2013;18:1090–1095.
11. Sullivan PF, Magnusson C, Reichenberg A, et al. Family history of schizophrenia and bipolar disorder as risk factors for autism. *Arch Gen Psychiatry*. 2012;69:1099–1103.
12. Carroll LS, Owen MJ. Genetic overlap between autism, schizophrenia and bipolar disorder. *Genome Med*. 2009;1:102.
13. Buchsbaum MS, Friedman J, Buchsbaum BR, et al. Diffusion tensor imaging in schizophrenia. *Biol Psychiatry*. 2006;60:1181–1187.
14. Karlsgodt KH, van Erp TG, Poldrack RA, Bearden CE, Nuechterlein KH, Cannon TD. Diffusion tensor imaging of the superior longitudinal fasciculus and working memory in recent-onset schizophrenia. *Biol Psychiatry*. 2008;63:512–518.
15. Sarrazin S, Poupon C, Linke J, et al. A multicenter tractography study of deep white matter tracts in bipolar I disorder: psychotic features and interhemispheric disconnectivity. *JAMA Psychiatry*. 2014;71:388–396.
16. Barnea-Goraly N, Kwon H, Menon V, Eliez S, Lotspeich L, Reiss AL. White matter structure in autism: preliminary evidence from diffusion tensor imaging. *Biol Psychiatry*. 2004;55:323–326.
17. Karlsgodt KH, Niendam TA, Bearden CE, Cannon TD. White matter integrity and prediction of social and role functioning in subjects at ultra-high risk for psychosis. *Biol Psychiatry*. 2009;66:562–569.
18. Luck D, Buchy L, Czechowska Y, et al. Fronto-temporal disconnectivity and clinical short-term outcome in first episode psychosis: a DTI-tractography study. *J Psychiatr Res*. 2011;45:369–377.
19. Carletti F, Woolley JB, Bhattacharyya S, et al. Alterations in white matter evident before the onset of psychosis. *Schizophr Bull*. 2012;38:1170–1179.
20. Yamada K, Matsuzawa H, Uchiyama M, Kwee IL, Nakada T. Brain developmental abnormalities in Prader–Willi syndrome detected by diffusion tensor imaging. *Pediatrics*. 2006;118:e442–e448.
21. White T, Nelson M, Lim KO. Diffusion tensor imaging in psychiatric disorders. *Top Magn Reson Imaging*. 2008;19:97–109.

22. White T, Schmidt M, Karatekin C. White matter 'potholes' in early-onset schizophrenia: a new approach to evaluate white matter microstructure using diffusion tensor imaging. *Psychiatry Res*. 2009;174:110–115.
23. White T, Ehrlich S, Ho BC, et al. Spatial characteristics of white matter abnormalities in schizophrenia. *Schizophr Bull*. 2013;39:1077–1086.
24. von Hohenberg CC, Pasternak O, Kubicki M, et al. White matter microstructure in individuals at clinical high risk of psychosis: a whole-brain diffusion tensor imaging study. *Schizophr Bull*. 2014;40:895–903.
25. Hoptman MJ, Nierenberg J, Bertisch HC, et al. A DTI study of white matter microstructure in individuals at high genetic risk for schizophrenia. *Schizophr Res*. 2008;106:115–124.
26. Festen DA, Wevers M, Lindgren AC, et al. Mental and motor development before and during growth hormone treatment in infants and toddlers with Prader–Willi syndrome. *Clin Endocrinol (Oxf)*. 2008;68:919–925.
27. Lukoshe A, Hokken-Koelega AC, van der Lugt A, White T. Reduced cortical complexity in children with Prader–Willi Syndrome and its association with cognitive impairment and developmental delay. *PLoS One*. 2014;9:e107320.
28. White T, El Marroun H, Nijs I, et al. Pediatric population-based neuroimaging and the Generation R Study: the intersection of developmental neuroscience and epidemiology. *Eur J Epidemiol*. 2013;28:99–111.
29. Smith SM, Jenkinson M, Johansen-Berg H, et al. Tract-based spatial statistics: voxelwise analysis of multi-subject diffusion data. *Neuroimage*. 2006;31:1487–1505.
30. Smith SM. Fast robust automated brain extraction. *Hum Brain Mapp*. 2002;17:143–155.
31. Mori S, Oishi K, Jiang H, et al. Stereotaxic white matter atlas based on diffusion tensor imaging in an ICBM template. *Neuroimage*. 2008;40:570–582.
32. Vogels A, Matthijs G, Legius E, Devriendt K, Fryns JP. Chromosome 15 maternal uniparental disomy and psychosis in Prader–Willi syndrome. *J Med Genet*. 2003;40:72–73.
33. Paus T, Collins DL, Evans AC, Leonard G, Pike B, Zijdenbos A. Maturation of white matter in the human brain: a review of magnetic resonance studies. *Brain Res Bull*. 2001;54:255–266.
34. Emery B. Regulation of oligodendrocyte differentiation and myelination. *Science*. 2010;330:779–782.
35. Judson MC, Sosa-Pagan JO, Del Cid WA, Han JE, Philpot BD. Allelic specificity of Ube3a expression in the mouse brain during postnatal development. *J Comp Neurol*. 2014;522:1874–1896.
36. Lu Y, Wang F, Li Y, Ferris J, Lee JA, Gao FB. The Drosophila homologue of the Angelman syndrome ubiquitin ligase regulates the formation of terminal dendritic branches. *Hum Mol Genet*. 2009;18:454–462.
37. Gibson EM, Purger D, Mount CW, et al. Neuronal activity promotes oligodendrogenesis and adaptive myelination in the mammalian brain. *Science*. 2014;344:1252304.
38. Bergles DE, Roberts JD, Somogyi P, Jahr CE. Glutamatergic synapses on oligodendrocyte precursor cells in the hippocampus. *Nature*. 2000;405:187–191.
39. Barres BA, Raff MC. Proliferation of oligodendrocyte precursor cells depends on electrical activity in axons. *Nature*. 1993;361:258–260.
40. Yu C, Li J, Liu Y, et al. White matter tract integrity and intelligence in patients with mental retardation and healthy adults. *Neuroimage*. 2008;40:1533–1541.
41. Alexander AL, Lee JE, Lazar M, Field AS. Diffusion tensor imaging of the brain. *Neurotherapeutics*. 2007;4:316–329.
42. Bennett IJ, Madden DJ, Vaidya CJ, Howard DV, Howard JH Jr. Age-related differences in multiple measures of white matter integrity: a diffusion tensor imaging study of healthy aging. *Hum Brain Mapp*. 2010;31:378–390.
43. Kumar R, Nguyen HD, Macey PM, Woo MA, Harper RM. Regional brain axial and radial diffusivity changes during development. *J Neurosci Res*. 2012;90:346–355.
44. Wheeler-Kingshott CA, Cercignani M. About "axial" and "radial" diffusivities. *Magn Reson Med*. 2009;61:1255–1260.
45. Lukoshe A, White T, Schmidt MN, van der Lugt A, Hokken-Koelega AC. Divergent structural brain abnormalities between different genetic subtypes of children with Prader–Willi syndrome. *J Neurodev Disord*. 2013;5:31.
46. Mozell RL, McMorris FA. Insulin-like growth factor I stimulates oligodendrocyte development and myelination in rat brain aggregate cultures. *J Neurosci Res*. 1991;30:382–390.
47. Almazan G, Honegger P, Matthieu JM, Guentert-Lauber B. Epidermal growth factor and bovine growth hormone stimulate differentiation and myelination of brain cell aggregates in culture. *Brain Res*. 1985;353:257–264.
48. Siemensma EP, Tummers-de Lind van Wijngaarden RF, Festen DA, et al. Beneficial effects of growth hormone treatment on cognition in children with Prader-Willi syndrome: a randomized controlled trial and longitudinal study. *J Clin Endocrinol Metab*. 2012;97:2307–2314.
49. Lo ST, Festen DA, Tummers-de Lind van Wijngaarden RF, et al. Beneficial effects of long-term growth hormone treatment on adaptive functioning in infants with Prader–Willi syndrome. *Am J Intellect Dev Disabil*. 2015;120:315–327.
50. Yeung MS, Zdunek S, Bergmann O, et al. Dynamics of oligodendrocyte generation and myelination in the human brain. *Cell*. 2014;159:766–774.
51. Mukherjee P, Miller JH, Shimony JS, et al. Diffusion-tensor MR imaging of gray and white matter development during normal human brain maturation. *AJNR Am J Neuroradiol*. 2002;23:1445–1456.